Measurement of the Mass Properties of Rigid Bodies by means of Multi-filar Pendulums - Influence of Test Rig Flexibility

Giorgio Previati[a], Massimiliano Gobbi[a], Gianpiero Mastinu[a]

[a] *Politecnico di Milano, Department of Mechanical Engineering, Via La Masa 1, Milan*

Abstract

Mass properties (mass, centre of gravity location and inertia tensor) are commonly defined as attributes of rigid bodies. The measurement of such attributes is usually performed under the hypothesis of rigid behaviour of both the body under test and the test rig. For large or heavy bodies, the forces exchanged between the body and the testing structure may be so high that the rigid behaviour hypothesis is not satisfied. The body under test can often be considered as rigid, so the accuracy of the measurement can be affected by the deformations of the testing structure.

In this paper, the effect of the deformation of the testing structure on the measurement of relatively large or heavy bodies is investigated both numerically and experimentally. The InTenso+ Measuring System of the Politecnico di Milano, a special type of multi-filar pendulum is considered relevant as example. A flexible multi-body model of the test rig is employed for assessing the influence of test rig deformations on mass properties measurement.

Experimental tests are conducted on a series of bodies to study the uncertainty. Numerical and experimental evidences show that the deformation of the testing structure can alter considerably the results of the measurement. However, this effect can be modelled with a reasonable accuracy. A proper mathe-

*Corresponding author
Email address: giorgio.previati@polimi.it (Giorgio Previati)
URL: www.mecc.polimi.it/en/ (Giorgio Previati)

matical procedure is developed for use during the measurement to compensate the effects of the undesired test rig deformations.

The presented procedure can be effectively employed when the mass properties of very large or heavy bodies have to be measured and the construction of a sufficiently rigid testing structure is impossible in practice.

Keywords: inertia property measurement, large bodies, flexible multi-body modelling

---

1. Introduction

In the literature, many papers can be found discussing different methods for the measurement of the mass properties (for a literature survey see [1, 2, 3]). The mass parameters are ten parameters, namely mass, centre of gravity location and inertia tensor (six parameters). Mass and centre of gravity location can be measured by static or dynamic procedures [1].

To measure the inertia tensor, a dynamic procedure is required [3]. A motion is given to the body under investigation, kinematic quantities or forces are measured and then the components of the inertia tensor are derived by a suitable mathematical procedure. Simple rotations around an axis fixed in the space, complex motions or vibrations can be used [1, 3]. In the first case, one component of the inertia tensor can be measured for each experiment [1, 3], in the other cases the full inertia tensor can be measured by a single test. In some special case, mass and centre of gravity location can be measured along with the inertia tensor components [1, 3].

In most of the available techniques, both the body under investigation and the test rig are considered as rigid bodies. Methods based on frequency domain data are able to distinguish between rigid and deformable modes of the body under investigation [4, 5, 6]. These methods, however, due to the very small motion of the body, have generally low accuracy in the measured values [1, 3].

In general, a test rig for the dynamic measurement of the mass properties, can be divided into three parts [7, 8]. A fixed frame, a carrying frame and

a linkage system. The carrying frame has the function to support the body under investigation. The fixed frame is a structure connecting the test rig to the ground. The carrying frame and the fixed frame are linked by a system that allows a relative motion. If all of such three components are rigid, i.e. their deformations are negligible, the motion of the body under investigation is a rigid body motion. The kinematics of the motion is related with the degrees of freedom allowed by the linkage system.

If one or more of the components of the test rig have a non negligible deformation, the resulting motion of the body will contain the rigid body motion and some additional vibrations due to the deformation of the test rig. Very few papers can be found in the literature considering the deformation of the test rig in the measuring process. Typically, these papers deal with elastic suspension methods, where the effects of the deformation of the soft springs connecting the carrying frame to the fixed frame is considered in the mathematical identification procedure [9, 10, 11].

For the measurement of large or heavy bodies, the stiffness of the test rig can be a critical issue. In order to accommodate large or heavy bodies, large or massive carrying frames have to be employed. Given that the carrying frame moves with the body, its inertia tensor is added to the inertia tensor of the body. In order to optimize the sensitivity of the test rig, the inertia of the carrying frame must be minimized. Therefore, for large or heavy bodies, the realization of a light and stiff carrying frame can be a very complex, if not impossible, task.

Therefore, a certain amount of deformation has to be expected in the carrying frame and, for very large or heavy bodies, even in the fixed frame. Some amount of deformation can be present also in the linking system. Some papers dealing with the measurement of mass properties of large or heavy bodies can be found. In [12] the measurement of a spaceship is described. In [13] a military truck is considered. [14] and [15] show different test rigs for the measurement of the inertia tensor of small airplanes, satellites and rockets. In none of these papers the deformation of the test rig is taken into account. In [8] a test rig for the accurate measurement of the inertia properties of aerospace vehicles is

presented. In this paper, the stiffness of the system is considered to be high enough to have negligible effects on the measured quantities.

In the present paper, a numerical and experimental study on the effect of the deformations of a test rig on the measured values of the location of the centre of gravity and of the components of the inertia tensor is presented. The InTenso+ Measurement System, developed at the Politecnico di Milano [7, 16, 2, 17], is taken as reference and used for the experimental tests.

The paper is organized as follows. The first section is devoted to a short description of the InTenso+ System. Then, a flexible multi-body model of the test rig is presented and used to numerically investigate the effects of the deformation of the test rig when relatively large or heavy bodies are measured. Finally, the measurements of the inertia properties of eighteen bodies are analysed to asses the influence of test rig flexibility.

2. InTenso+ System

The InTenso+ System is a method for the measurement of the mass properties of rigid bodies developed at the Politecnico di Milano (Technical University of Milan) and is described in detail in [7].

Fig.1 shows the scheme of the InTenso+ System. The test rig is a multi-filar pendulum in which the cables are replaced by rods. The body under investigation is located on a carrying frame connected to a fixed frame by means of three or four rods. Low friction Hooke's joints allow the relative motion between rods, fixed frame and carrying frame. The motion of the system is obtained by displacing the carrying frame from the equilibrium position. The motion and the forces acting on the carrying frame are recorded and the coordinates of the centre of gravity and the inertia tensor components are computed by a proper mathematical procedure. In Fig.2, the two test rigs currently available are shown.

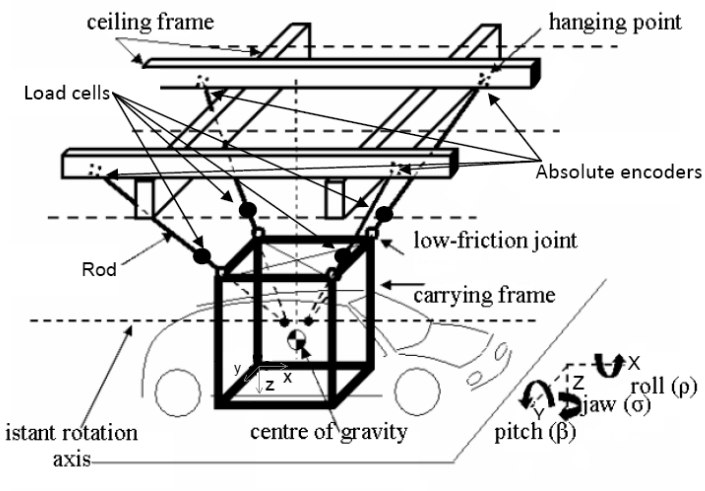

Figure 1: Scheme of the InTenso+ rig for measuring the inertia tensor of rigid bodies (such as vehicles). The local (small letters) and global (capital letters) reference systems are reported. Adapted from [7].

Figure 2: Left: InTenso+ test rig for rigid bodies up to 3500 kg. Right: InTensino+ test rig for relatively light and compact rigid bodies (up to 400 kg).

2.1. Mass properties measurement

The mathematical model for the measurement of the inertia properties of a rigid body by using the InTenso+ System are fully described in [7]. In this section, the used approach is briefly summarized.

The identification of the inertia properties is based on the measurement of the motion of the body and on the reaction forces along the rods. The general expression of the second Newton's law can be expressed, with respect to a reference point P, as [1, 7]

$$\boldsymbol{f} = \mathbf{M}\left(m, \boldsymbol{X}_{\mathrm{G}}, \mathbf{J}, \boldsymbol{\Theta}, \boldsymbol{\omega}\right) \cdot \boldsymbol{a}_{\mathrm{P}} \tag{1}$$

where $\boldsymbol{f}$ is the vector of the generalized forces acting on the body, $\mathbf{M}$ is the mass matrix (function of the mass (m), of the location of the centre of gravity with respect to the reference point P ($\boldsymbol{X}_{\mathrm{G}}$), of the inertia tensor ($\mathbf{J}$) and of the state of the body ($\boldsymbol{\Theta}$, $\boldsymbol{\omega}$)) and $\boldsymbol{a}_{\mathrm{P}}$ is the vector of the linear acceleration of the reference point P.

Eq. 1 can be rewritten in a suitable form for the identification of the mass properties as [1, 7]

$$\underbrace{\boldsymbol{f}_{6\times1} - \begin{bmatrix} m \cdot \boldsymbol{a}_{\mathrm{P},3\times1} \\ \mathbf{0}_{3\times1} \end{bmatrix}}_{\boldsymbol{b}_{6\times1}} = \underbrace{\begin{bmatrix} \mathbf{g}\left(m, \boldsymbol{\Theta}, \boldsymbol{\omega}, \dot{\boldsymbol{\omega}}\right)_{3\times3} & \mathbf{0}_{3\times3} \\ \mathbf{h}\left(m, \boldsymbol{\Theta}, \boldsymbol{\omega}, \dot{\boldsymbol{\omega}}\right)_{3\times6} & \mathbf{k}\left(\boldsymbol{\Theta}, \boldsymbol{\omega}, \dot{\boldsymbol{\omega}}\right)_{3\times6} \end{bmatrix}}_{\mathbf{a}_{6\times9}} \cdot \underbrace{\begin{bmatrix} \boldsymbol{X}_{\mathrm{G},3\times1} \\ \boldsymbol{J}_{6\times1} \end{bmatrix}}_{\boldsymbol{x}_{9\times1}} \tag{2}$$

being $\boldsymbol{J} = \left[J_{xx} J_{yy} J_{zz} J_{xy} J_{xz} J_{yz}\right]^T$ the vector of the components of the inertia tensor (inertia tensor definition in Appendix A).

Vector $\boldsymbol{b}$ collects the forces (reaction forces plus inertial forces) acting on the body translated to point P and the translation moments. Matrix $\mathbf{a}$ is the coefficient matrix and is function of the mass and of the state (described by angular positions, velocities and accelerations) of the system. The terms in $\mathbf{a}$ and $\boldsymbol{b}$ have to be measured.

The nine unknowns (three coordinates of the centre of gravity with respect to the reference point P and six terms of the inertia tensor) are collected in vector

$\boldsymbol{x}$. As a result, the system of eq. 2 has nine unknowns and six equations. At least two different time instants have to be considered to solve the system. If n different time instants are considered, from eq. 2, the following overdetermined system can be written

$$\begin{bmatrix} \boldsymbol{b}_1 \\ \boldsymbol{b}_2 \\ \vdots \\ \boldsymbol{b}_i \\ \vdots \\ \boldsymbol{b}_n \end{bmatrix} = \begin{bmatrix} \mathbf{a}_1 \\ \mathbf{a}_2 \\ \vdots \\ \mathbf{a}_i \\ \vdots \\ \mathbf{a}_n \end{bmatrix} \cdot \boldsymbol{x} \qquad \Longrightarrow \qquad \boldsymbol{B} = \mathbf{A} \cdot \boldsymbol{x} \tag{3}$$

The system of eq. 3 can be solved by the least squares method

$$\boldsymbol{x} = \mathbf{A}^{\dagger} \cdot \boldsymbol{B} \tag{4}$$

where $\mathbf{A}^{\dagger}$ is the pseudo-inverse of $\mathbf{A}$ [18].

2.2. Instrumentation

In order to build matrices $\mathbf{A}$ and $\boldsymbol{B}$ of eq. 3, the reaction forces along the rods and the kinematics of the system composed by the carrying frame and body under investigation have to be measured.

The forces acting along the rods are measured by z-folded load cells positioned between the rods and the Hookes joints on the carrying frame.

The kinematics of the system is reconstructed from the measurement of the rotation of the Hook's joints between the fixed frame and the rods. For each Hooke's joint, two absolute encoders are employed to measure the rotation of the two axes of the joint. From these rotations, knowing the lengths of the rods, the spatial position of the centres of the Hook's joint between the carrying frame and the rods is computed. From these positions, the rotation angles of the carrying frame are calculated according to the procedure described in [7]. Finally, by derivation, also angular velocities and accelerations are obtained.

This procedure guarantees a sufficient level of accuracy in the description of the kinematics of this application (see [7] for the experimental proof).

It can be observed that the stiffness of the test rig influences the process. The loads along the rods can present higher frequencies contribution due to the deformation of the components of the test rig. The reconstruction of the kinematics is based on the lengths of the rods and the locations of the Hooke's joint on the fixed and carrying frames. All these geometrical quantities change when the test rig exibits deformations.

2.3. Static procedure for measuring the centre of gravity location

A static procedure is also available for the measurement of the in plane coordinates (x and y coordinates in Fig. 1) of the centre of gravity in case the InTenso+ test rig is employed. For this test rig, the carrying frame is a cage (Fig. 2 left) in which the body under investigation is positioned. Below the bottom part of the cage, a knife edge can be positioned parallel to the x or y axis. The cage is then positioned on the knife edge and by measuring the restoring force required to keep the system in equilibrium over the knife edge, the two centre of gravity coordinates can be measured with a good accuracy. Since this method is simple and accurate, it is the usual adopted procedure. The measured values of the in plane coordinates of the centre of gravity are then introduced in eq. 2 and the system is rearranged in order to identify only the remaining seven unknown mass properties, i.e the height of the centre of gravity and the six terms of the inertia tensor.

In the configuration used for the experimental tests reported in this paper, the InTenso+ test rig has an accuracy of 3% on the measurement of the moments of inertia (MOI) and of 1.5% (referred to the value of the maximum MOI) on the measurement of the products of inertia (POI). These percentages refer to a 2σ interval, representing the 95% confidence interval. The accuracy on the measurement of the centre of gravity is $\pm 3mm$ in the plane (static method). The accuracy on the height of the centre of gravity is $\pm 5mm$.

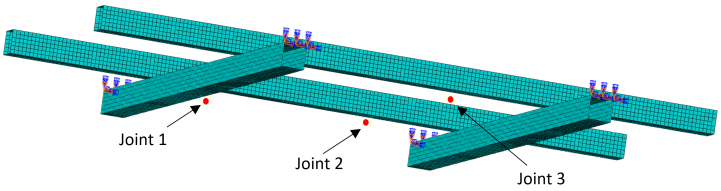

Figure 3: Finite element model of the fixed frame. The four supporting beams are meshed by quadratic quadrilateral elements and the Hook's joint centres are connected to the structure by rigid couplings.

3. Flexible multi-body model of the test rig

A flexible multi-body model of the test rig has been constructed by using Matlab Simmechanics^{TM}. The procedure for constructing a flexible multibody model by using this toolbox is explained in the Mathworks reference site [19]. The complete description of the model of the test rig can be found in [17] and it is summarized in this section.

The flexibility of the test rig is included in the model by considering the deformation of the carrying frame and of the fixed frame. The deformation of the carring frame is described by superimposing the deformation of the body to its rigid motion. For the fixed frame, the deformation of the body is computed and the motion of the hanging points (joints 1, 2 and 3 of Fig.3) is derived. For the two bodies, the same mathematical approach is used. The deformation of the body is computed by a state-space model defined as

$$\begin{cases} \dot{\boldsymbol{x}} = \mathbf{A}\boldsymbol{x} + \mathbf{B}\boldsymbol{u} \\ \boldsymbol{y} = \mathbf{C}\boldsymbol{x} + \mathbf{D}\boldsymbol{u} \end{cases} \tag{5}$$

where $\mathbf{A}$, $\mathbf{B}$, $\mathbf{C}$ and $\mathbf{D}$ are the state matrices, $\boldsymbol{x}$ is the vector of the state variables with time derivatives $\dot{\boldsymbol{x}}$, $\boldsymbol{u}$ is the vector of the inputs and $\boldsymbol{y}$ the vector of the outputs.

Matrix $\mathbf{A}$ contains the reduced mass, stiffness and damping matrices of each considered body. The reduced mass and stiffness matrices have been computed

by considering a finite element model of the two bodies. The finite element models, realized by using ABAQUS 6.14 [20], are reported in Fig. 3 and Fig. 4 for the fixed and carrying frames respectively. For both bodies, the joint locations represent the centres of the Hook's joints. The three displacements of these points are the retained degrees of freedom and represent the interface of the bodies with the model of the system.

The reduced damping matrix has been computed form the mass and stiffness matrices by considering a Rayleigh structural damping [21]. The parameters of the structural damping have been set in order to obtain a damping equal to the 2% of the critical damping. To compute the matrix coefficients, the first and third eigenmode of the structures have been considered as explained in [21]. The damping refers only to the deformation of the structures, the very small damping of the large motion of the pendulum is neglected.

When dealing with dynamic models, to achieve a better accuracy in the dynamic simulations, a certain number of flexible modes can be included into the reduced stiffness and mass matrices of system [22]. In the present case, different simulations have been performed considering up to 6 flexible modes for the two frames. Given the relative low frequency of the motion of the system (well below the first eigenfrequencies of the two frames), no appreciable difference has been found if the flexible modes were considered or not. Therefore, in the following, only the static reduction [23] is considered in the model.

4. Experimental results

In this section the experiments realized by using the InTenso+ test rig to asses the effect of the compliance of the test rig on the measurement of the mass properties are presented. The experiments have been completed by considering 18 vehicles with mass ranging from 1500 kg to 2500 kg. In table 1, the mass properties ranges referring to the system vehicle + carrying frame are reported.

For the measurement of the mass properties, two different measurement algorithms have been used. The first algorithm, based on eq. 4 and called

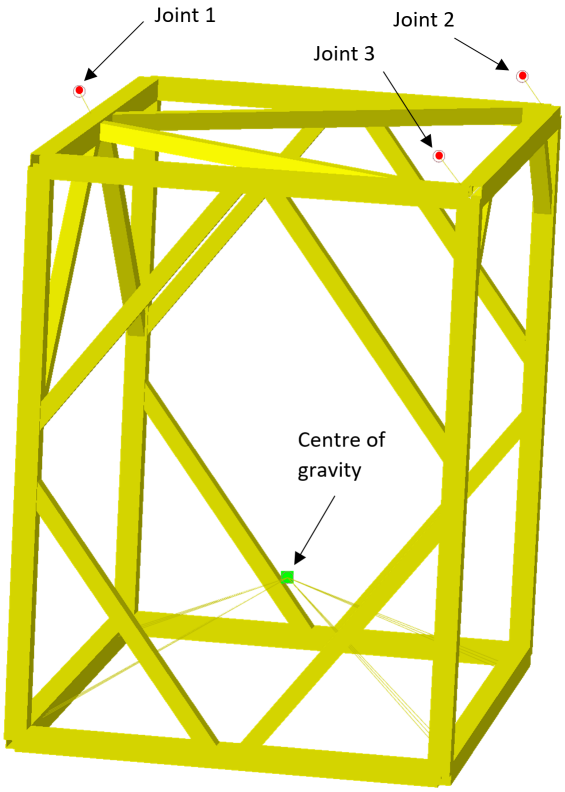

Figure 4: Finite element model of the carrying frame. The carrying frame is meshed with beams and constrained in the centre of gravity of the system composed by the carrying frame and the body under consideration.

Table 1: Data ranges for the 18 considered vehicles. Data refers to the system vehicle + carrying frame

	Minimum	**Maximum**
Mass [kg]	2000	2950
CoG Height [mm](*)	-765	-570
J_{xx} [kgm^2]	1200	1650
J_{yy} [kgm^2]	2250	5750
J_{zz} [kgm^2]	2300	5550
J_{xy} [kgm^2]	-5	45
J_{xz} [kgm^2]	-485	185
J_{zz} [kgm^2]	-10	5

(*) With respect to the carrying frame reference system.

rigid measurement algorithm, considers all the components of the system as rigid, matrix a_i in eq. 3 refers to a multi-body system (rigid bodies). The second algorithm, called flexible measurement algorithm, considers the flexible characteristic of the different parts of the test rig to build matrix a_i in eq. 3. Both of the algorithms use the same measured data. The deformations of the fixed frame, of the carrying fame and of he connecting bars are computed as shown in section 3.

To assess the variance of the measurements, for each vehicle, the measurement has been repeated between 8 to 18 times. The total number of measurements is 197. Each measurement is obtained by considering a set of 6 time histories of the motion of the test rig starting from different initial conditions. The use of six different motions guarantees a good conditioning of the solving system as explained in [7].

4.1. Height of the centre of gravity

A static procedure has been used for the measurement of the height of the centre of gravity. The procedure consists in tilting the carrying frame and deriving the height of gravity height from the measurement of the tilting angle and

of the required force. The accuracy of such measurement is $\pm 7mm$. Additionally, the two measurement algorithms (flexible and rigid) have been exploited to derive the centre of gravity height. The parameter values obtained with the static procedure are taken as reference. In Fig. 5 probability charts are shown referring to discrepancies between measurements performed with rigid and flexible algorithm. Discrepancies are given as differences with respect to references values, measured by the static procedure.

Referring to the flexible measurement algorithm, the distribution of the differences of the measured values with respect to the reference values has mean equal to -0.6 mm and standard deviation equal to 4.9 mm. The experimental points fit very well on the straight line representing the theoretical normal distribution. The results show that the flexible measurement algorithm agrees very well with the static measurement procedure. In fact, the distribution of the differences has a almost null mean value and the standard deviation is close to the combination of the two standard deviations of the involved measuring procedures ($\sigma = 2.5mm$ for the dynamic procedure and $\sigma = 3.5mm$ for the static procedure, the theoretical combination is $\sigma = 4.3mm$).

A totally different situation has been found for the rigid measurement algorithm. In this case, the distribution of the differences of the measured values has mean value equal to 45.1 mm and standard deviation equal to 41.4 mm and the points do not fit the theoretical normal distribution. These results show that neglecting the compliance of the test rig leads to completely erratic measurements of the height of the centre of gravity.

4.2. Inertia tensor components

In this section, the values of the components of the inertia tensor measured by using the flexible or rigid algorithms are compared. Fig. 6 reports, for each component of the inertia tensor, the number of bodies for which the two algorithms have given the same result. Fig. 6 has been constructed as follows. The measurement on each body has been repeated between 8 to 18 times. For each measurement of a component of the inertia tensor, the distribution of the

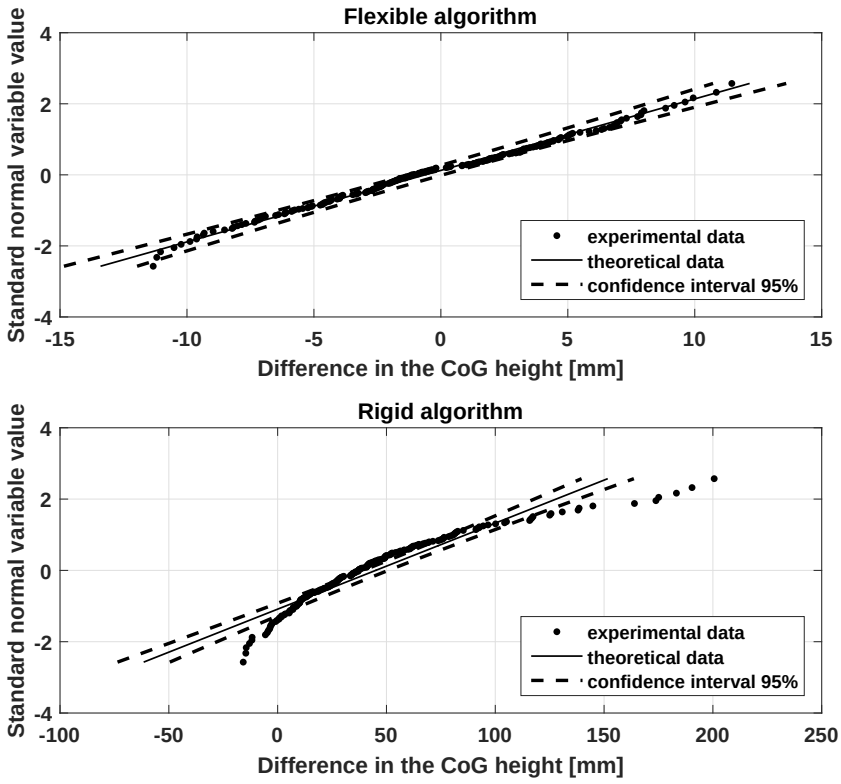

Figure 5: Normal probability chart of the measurement of the height of the centre of gravity (CoG). Top: flexible measurement algorithm. Bottom: rigid measurement algorithm. Reference values refer to measurements performed by a static procedure.

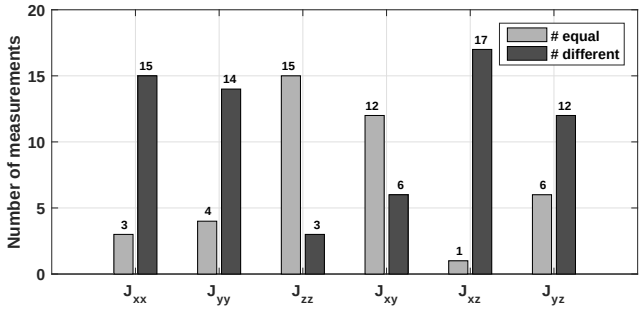

Figure 6: Comparison between the measured values of the component of the inertia tensor by considering or not the compliance of the test rig. Two measured values are considered different according to the Welch's t-test [24] with 0.05 significance level.

measured values has been computed. Then, for each component of the tensor and for each body, a Welch's t-test has been performed with a significance level of 0.05 [24]. The hypothesis of the test has been that the two distributions were equal, the alternative hypothesis that were different.

By inspecting Fig. 6, it can be noticed that the greater differences have been shown in the components of the inertia tensor that are correlated with the height of the centre of gravity (z coordinate in the local reference system of Fig. 1), i.e. J_{xx}, J_{yy}. From this observation, and by remembering the large errors in the measurement of the centre of gravity height of the rigid alghoritm (Fig. 5), one may relate these differences to the differences in the measurement of the height of the centre of gravity .

To understand if the differences in the measurements of the components of the inertia tensor reported in Fig. 6 are due to the propagation of the error in the centre of gravity height measurement or to the deformation of the test rig, a second comparison is reported in Fig. 7. In this figure, the Welch's t-test has been performed between the values of the inertia tensor identified by the flexible algorithm and the ones identified by a modified version of the rigid algorithm. In this version, the height of the centre of gravity is not estimated but imposed equal to the value measured by the static procedure. From Fig. 7, it can be

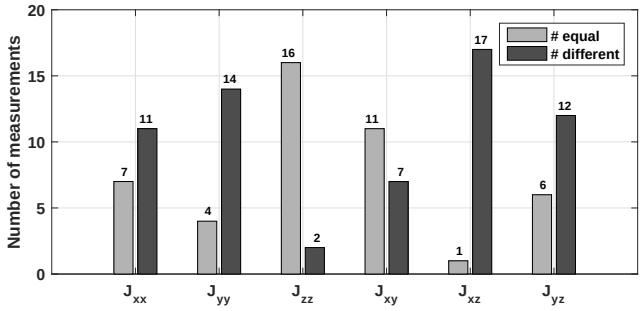

Figure 7: Comparison between the measured values of the component of the inertia tensor by considering or not the compliance of the test rig. In this figure, for the rigid algorithm, the value of the height of the centre of gravity measured by the static method has been used. Two measured values are considered different according to the Welch's t-test [24] with 0.05 significance level.

observed that the results are very similar to the ones shown in Fig. 6, meaning that the compliance of the test rig actually plays a very important role in the identification of the terms of the inertia tensor.

Fig. 8 shows the percentage of tests within the 2σ accuracy of the test rig (Sect. 2.3). The flexible algorithm is globally well above te 95% of tests that represents the 2σ threshold. The rigid algorithm shows much worse performances, especially on the measurement of the principal components of the tensor.

The compliance of the test rig has effects not only on changing the measured values, but also on reducing the repeatability of the measurement.

5. Numerical analysis

In this section, the flexible multi-body model of the test rig is used to simulate the measurement process. A reference body (data in table 2) has been chosen among the ones tested on the test rig. The body is one of the heaviest ever tested. For such a body a large influence of the test rig stiffness on the measurement of mass properties was experienced.

In the next subsection, the flexible multi-body model of the test rig is vali-

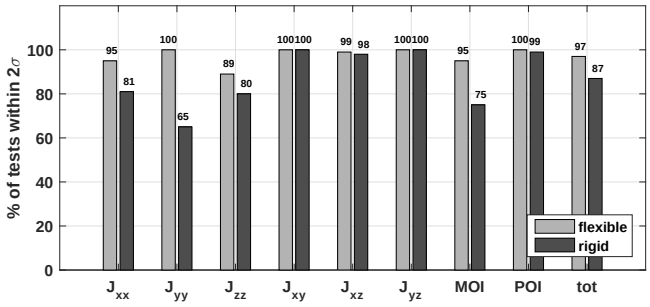

Figure 8: Percentage of tests within the 2σ interval of the test rig for the flexible and rigid identification algorithms. The total number of tests is 197.

dated by reproducing nine experiments for the measurement of the inertia properties of the light truck and comparing the standard deviation computed by the model and the standard deviations obtained from the experiments. Then, in the following subsection, a sensitivity analysis is performed to understand the relationship between the inertial properties of the body under investigation and test rig stiffness for requiring the modelling of the compliance of the system.

5.1. Model validation

The model validation is performed as follows.

- The same number of sets of six time histories used for measuring the inertia properties of the light truck are simulated by using the flexible multi-body model of the test rig. For each time history, the output of the virtual instrumentation is saved in the same format of the actual experimental data measured by the test rig. Each time history has been generated starting from a random set of initial conditions. The considered number of sets of time histories is nine.

- The rigid identification algorithm is employed to identify the values of the inertia properties of the system carrying frame and vehicle from the simulated data. No uncertainty on the geometry of the test rig or noise

Table 2: Nominal mass properties of a reference body (composed by a light truck and by the carrying frame).

Mass	[kg]	2914
CoG longitudinal coord. (x) $^{(*)}$	[mm]	511
CoG lateral coord. (y) $^{(*)}$	[mm]	-8
CoG height (z) $^{(*)}$	[mm]	-598
J_{xx}	[kgm^2]	1632
J_{yy}	[kgm^2]	5729
J_{zz}	[kgm^2]	5510
J_{xy}	[kgm^2]	44
J_{xz}	[kgm^2]	-483
J_{zz}	[kgm^2]	4

$^{(*)}$ With respect to the carrying frame reference system.

in the measured signal is considered. The only source of error is the deformation of the test rig.

- The results of the simulations are compared with the results of the actual measurements on the vehicle.

It must be observed that to avoid the excitation of flexible motions, both the real test rig and the numerical model have to be displaced from rest with a very smooth movement. In the real test rig, such displacement is given by a human operator that cannot be modelled, hence the numerical model cannot have the same initial conditions. As a result, since the system is non linear, the use of different initial conditions leads to different motions of the system. In this situation, the one to one comparison of each numerical test with each experimental test cannot be performed. However, the use of nine sets of six different time histories allows for a statistical comparison between numerical and experimental tests.

Fig. 9 shows the normal probability plots for the measured values of the height of the centre of gravity by using the rigid and the flexible algorithm

along with the measured values of the parameter obtained by the numerical simulations. The value of the z coordinate measured by the static tilting method is -598±7 mm (which is also the reference value for the simulations, see table 2). It can be observed from the experimental data that if the deformations of the test rig are neglected, the values of the centre of gravity shows a much large scatter. The mean values of the two identification algorithms are different with the mean value of the flexible identification algorithm coinciding with the value measured by the static tilting method. The simulations pretty well reproduce the scatter of the measures performed by using the rigid algorithm. Also the mean values of the measured obtained by the rigid algorithm and the simulations are similar (-614 mm and -620 mm, respectively).

Fig. 10 shows the normal probability plots for the experimentally measured values of J_{yy} by using the two identification algorithms along with the simulated distribution. Referring to the experimental data, neglecting the stiffness of the test rig leads to a mush larger dispersion of the measurements and to an appreciable difference in their mean value (-0.4%). The numerical model reproduces well the experimental dispersion (0.80% experimental, 0.75% numerical) and overestimates the mean error (-1.2%).

For the purposes of the following sensitivity analysis, the numerical model is able to catch the main effects of the stiffness of the test rig on the measurement of the height of the centre of gravity and on the considered term of the inertia tensor with a sufficient level of accuracy.

5.2. Sensitivity analysis

In Fig. 11 a comparisons between the pitch angular acceleration (Fig. 11 top) and the forces on the central rod (Fig. 11 bottom) simulated starting from the same initial conditions by a rigid multi-body model of the system (i.e. the same model of section 3 where the flexible elements have been replaced by rigid elements) and by the flexible multi-body model is shown. Pitch angular acceleration shows that the flexibility of the system can influence both the amplitude and the frequency of the motion. The analysis of the bottom part of Fig. 11

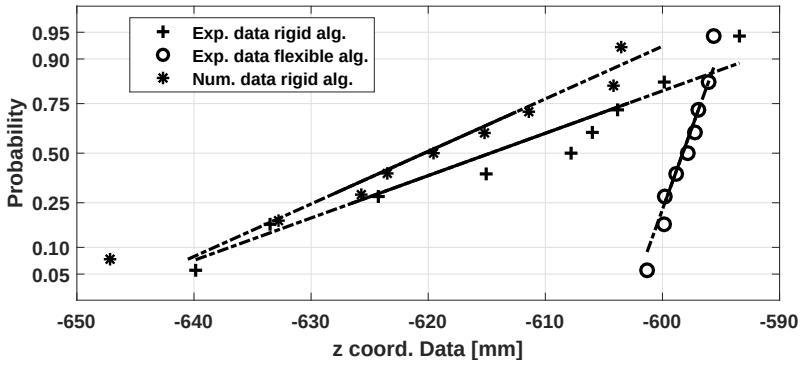

Figure 9: Normal probability plots for the measured values of the z coordinate of the centre of gravity. Crosses: experimental data and rigid identification algorithm. Circles: experimental data and flexible identification algorithm. Asterisks: numerical data and rigid identification algorithm.

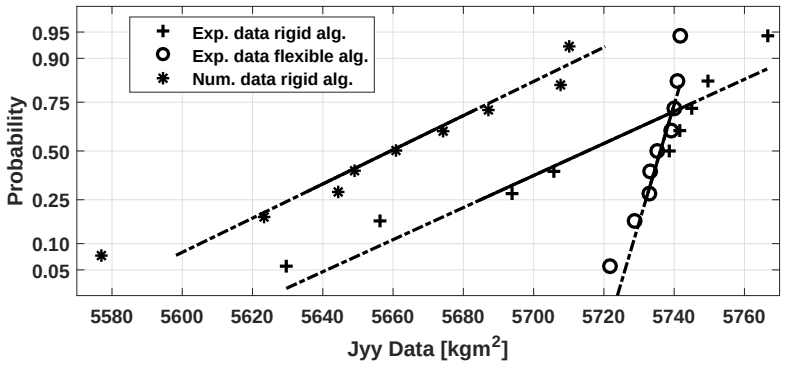

Figure 10: Normal probability plots for the measured values of the J_{yy} coordinate of the centre of gravity. Crosses: experimental data and rigid identification algorithm. Circles: experimental data and flexible identification algorithm. Asterisks: numerical data and rigid identification algorithm.

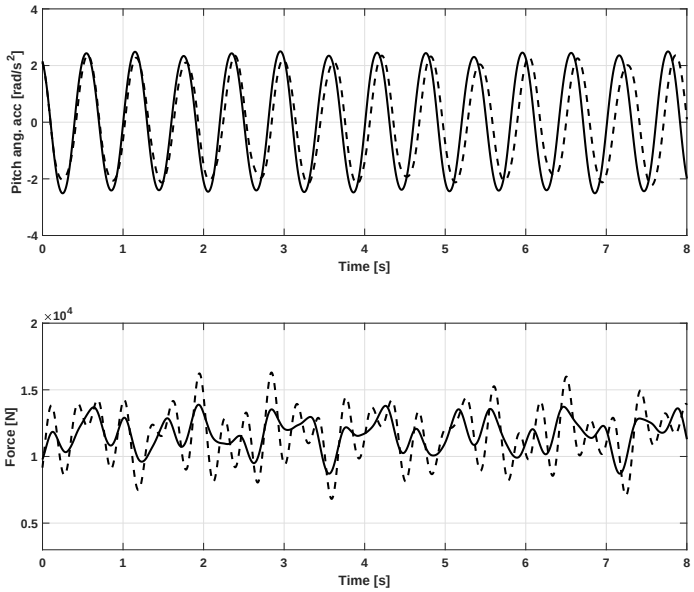

Figure 11: Comparison of simulated time histories starting from the same initial condition by model A and E of table 3. Top: pitch angular acceleration. Bottom: force along the central connecting bar. Solid line: rigid model. Dashed line: flexible model. Data in table 2.

shows that the flexibility of the system introduces higher frequency terms in the reaction forces along the connecting rods. All these effects, along with the geometrical variations of the test rig, have to be taken into account to correctly identify the inertia properties of the body under investigation.

To avoid such a different behaviour between the rigid and the flexible models, either the mass of the system carrying frame plus body under investigation has to be reduced or the stiffness of the test rig has to be increased. In the following two analyses are performed. In the first analysis, the mass of the system carrying frame plus body under investigation is reduced from its nominal value to the 10% of the value while keeping the stiffness constant at its nominal value. As the mass is reduced, the terms of the inertia tensor are reduced with the same ratio. In the second analysis, mass and inertia are kept constant at their nominal values

while the stiffness of the fixed frame, carrying frame and rods are increased of the same amount from their nominal value to ten times these value.

In Fig. 12 and Fig. 13, the results of the two analyses on the measurement of the height of the centre of gravity and of the pitch moment of inertia are reported. Fig. 12 shows the mean measurement error as function of the first eigenfrequency of the system and Fig. 13 shows the standard deviations of the measurement as function of the first eigenfrequency of the system. In both figures, a clear trend can be seen. Mean errors and standard deviations are quite acceptable when the first eigenfrequency is above 6 Hz. For lower values of the first eigenfrequency, mean errors and standard deviations rapidly grow. It is interesting that the same behaviour is present both when varying mass and when varying stiffness. The leading quantity seems to be the first eigenfrequency of the system.

The higher frequency of the motion of the system is between 1.5 an 2 Hz. If the first eignfrequency is high enough (3 to 4 times) there is no interaction and the measurement is accurate even if the stiffness is neglected. When the first eigenfrequency is closer to the frequency of the motion of the system, the deformable modes and the system motion interact and this interaction has to be taken into account.

6. Conclusion

The paper has been devoted to the analysis of the effects of the stiffness of multi-filar pendulums on the measurement of the mass properties of rigid bodies. The InTenso+ System for the measurement of the mass properties of rigid bodies has been used as a reference test rig for the analysis.

In the first part of the paper, after the presentation of the InTenso+ System, a vast experimental campaign, comprising about two-hundred measurements of the mass properties of different bodies, has been reported. The tests have involved 18 bodies and each body has been measured from 8 to 18 times to assess mean values and standard deviations of the measurements.

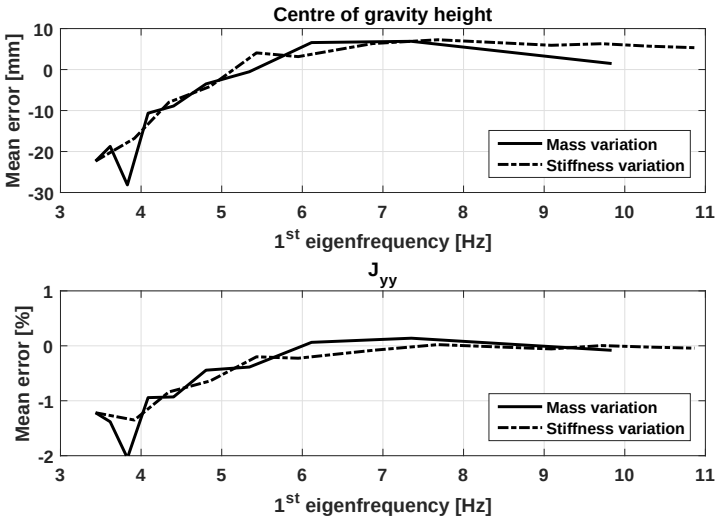

Figure 12: Mean error as function of the first eighenfrequency of the system. Continuous line: mass variation. Dash-dotted line: stiffness variation.

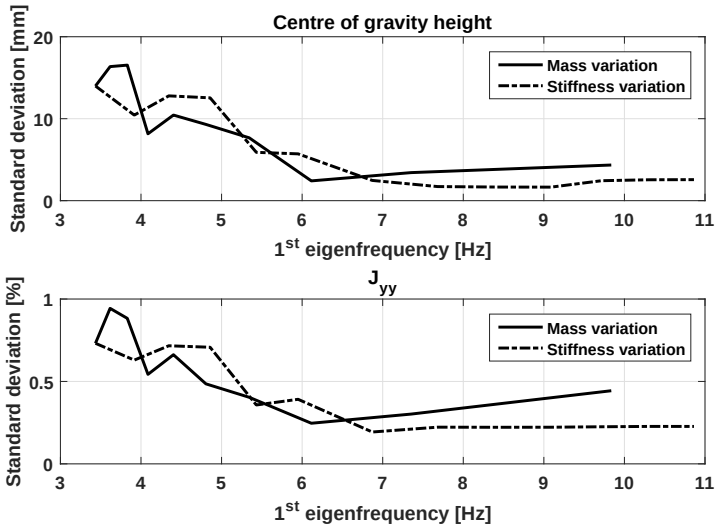

Figure 13: Standard deviation of the measurements as function of the first eighenfrequency of the system. Continuous line: mass variation. Dash-dotted line: stiffness variation.

The experimental results have shown that the measurement of the height of the centre of gravity can be greatly affected by the stiffness of the test rig. If the stiffness is neglected in the measuring procedure, errors up of the order of 10-20% of a characteristic dimension of the body can be found. Conversely, if the stiffness is taken into account, the value of the height of the centre of gravity can be measured within an uncertainty of less than 1% of said characteristic dimension.

Referring to the measurement of the terms of the inertia tensor, neglecting the stiffness of the test rig leads to a statistically different measurement with respect to taking the stiffness into account in the 62% of the performed measurements. Moreover, the repeatability of the measurement is worsened. In fact, when the stiffness is taken into account, the measurements is in the 2σ accuracy of the test rig in the 97% of the cases. This percentage reduces to the 87% if the stiffness is neglected.

In the second part of the paper, a flexible multi-body model of the test rig is presented. The model is validated against the available data and is able to get the main effects of stiffness on the measurement. A light truck has been taken as reference to perform a sensitivity analysis aimed to assessing the value of stiffness of the test rig and of the inertia properties of the body under investigation that allow for neglecting the flexibility effects.

It turned out that the eigenfrequency of the first deformation mode of the pendolum is a good indicator of the status of the testing. If the first eigenfrequency is higher than 3 or 4 times the frequency of the motion of the system, a good accuracy can be obtained even if the stiffness of the test rig is totally neglected. For lower values of the the eigenfrequency of the first deformation mode, the stiffness of the test rig has to be considered in the measurement procedure.

References

[1] C. Schedlinski, M. Link, Survey of current inertia parameter identification methods, Mechanical Systems and Signal Processing 15 (1) (2001) 189–211. doi:10.1006/mssp.2000.1345.
URL http://dx.doi.org/10.1006/mssp.2000.1345

[2] G. Previati, M. Gobbi, G. Mastinu, Improved Measurement Method for the Identification of the Centre of Gravity Location and of the Inertia Tensor of Rigid Bodies, in: 2008 Proceedings of the ASME International Design Engineering Technical Conferences and Computers and Information in Engineering Conference, DETC 2008, Vol. 5, ASME, 2008, pp. 841–850. doi:10.1115/DETC2008-49830.

[3] G. Previati, M. Gobbi, G. Mastinu, Measurement of the inertia tensor - A review, in: 73rd Annual Conference of the Society of Allied Weight Engineers, Inc., SAWE 2014, Society of Allied Weight Engineers, 2014, pp. 1–23.

[4] S. Pandit, Z.-Q. Hu, Determination Of Rigid Body Characteristics From Time Domain Modal Test Data, Journal of Sound and Vibration 177 (1) (1994) 31–41. doi:10.1006/jsvi.1994.1414.
URL http://www.sciencedirect.com/science/article/pii/S0022460X84714143

[5] R. A. B. Almeida, A. P. V. Urgueira, N. M. M. Maia, Identification of rigid body properties from vibration measurements, Journal of Sound and Vibration 299 (4-5) (2007) 884–899. doi:10.1016/j.jsv.2006.07.043.

[6] A. Malekjafarian, M. R. Ashory, M. M. Khatibi, Identification of inertia properties from the results of output-only modal analysis, Archive of Applied Mechanics 83 (6) (2013) 923–937. doi:10.1007/s00419-012-0727-0.

[7] M. Gobbi, G. Mastinu, G. Previati, A method for measuring the inertia properties of rigid bodies, Mechanical Systems and Signal Processing 25 (1) (2011) 305–318. doi:10.1016/j.ymssp.2010.09.004.

[8] R. S. Boynton, K. Wiener, A new high accuracy instrument for measuring moment of inertia and center of gravity, SAWE technical paper n.1827 (1988) 1–17.

[9] R. Kloepper, M. Okuma, Experimental identification of rigid body inertia properties using single-rotor unbalance excitation, Proceedings of the Institution of Mechanical Engineers, Part K: Journal of Multi-body Dynamics 223 (4) (2009) 293–308. doi:10.1243/14644193JMBD200.

[10] R. Klöpper, M. Okuma, J. Krüger, A new process for measuring complete inertia properties, MTZ worldwide 3.

[11] R. Kloepper, J. Bienert, M. Okuma, A Compact Device for Measuring Rigid-Body Properties Based on Five Unscaled Modes, in: IMAC proceedings, Orlando, FL, USA, 2014, pp. 215–224. doi:https://doi.org/10.1007/978-3-319-04753-9_22.

[12] W. L. Peterson, Mass Properties Measurement in the X-38 Project, SAWE technical paper n.3325 (2004) 1–19.

[13] D. A. Andreatta, G. J. Heydinger, R. A. Bixel, D. A. Coovert, Inertia Measurements of Large Military Vehicles, SAE techinical paper n. 2001-01-0792 (2001) 1–9doi:10.4271/2001-01-0792.

[14] R. C. De Jong, J. a. Mulder, Accurate estimation of aircraft inertia characteristics from a single suspension experiment (1987). doi:10.2514/3.45454.

[15] I. O. MacConochie, Measuring moments of inertia of aircraft and spacecraft, SAWE technical paper n.2126 (1993) 1–11.

[16] G. Previati, M. Gobbi, G. Mastinu, Method for the Measurement of the Inertia Properties of Bodies with Aerofoils, Journal of Aircraft 49 (2) (2012) 444–452. doi:10.2514/1.C031369.

[17] G. Previati, M. Gobbi, F. Ballo, Effect of the deformation of the supporting structure on the measurement of the inertia properties of vehicles, in: Proceedings of the ASME Design Engineering Technical Conference, American Society of Mechanical Engineers (ASME), 2016, pp. 1–10. doi:10.1115/DETC2016-59823.
URL http://proceedings.asmedigitalcollection.asme.org/proceeding.aspx?doi=10.1115/DETC2016-59823http://www.asmedl.org/journals/doc/ASMEDL-home/proc/

[18] Å. Björck, Numerical methods for least squares problems, Society for Industrial and Applied Mathematics, Philadelphia U.S.A., 1996.

[19] V. Chudnovsky, A. Mukherjee, J. Wendlandt, D. Kennedy, Modeling Flexible Bodies in SimMechanics (2006).
URL http://www.mathworks.com/company/newsletters/articles/modeling-flexible-bodies-in-simmechanics-and-simulink.html?s{_}tid=gn{_}loc{_}drop

[20] Simulia, ABAQUS Analysis User's Guide, ver. 6.14, 2014.

[21] I. Chowdhury, S. P. Dasgupta, Computation of Rayleigh damping coefficients for large systems, Electronic Journal of Geotechnical Engineering 8 (2003) 1–11.

[22] D. de Klerk, D. J. Rixen, S. N. Voormeeren, General Framework for Dynamic Substructuring: History, Review and Classification of Techniques, AIAA Journal 46 (5) (2008) 1169–1181. doi:10.2514/1.33274.

[23] R. Guyan, Reduction of stiffness and mass matrices, AIAA Journal 3 (2) (1964) 380.

[24] G. D. Ruxton, The unequal variance t-test is an underused alternative to Student's t-test and the Mann-Whitney U test, Behavioral Ecology 17 (4) (2006) 688–690. doi:10.1093/beheco/ark016.

Appendix A. Definition of the inertia tensor

The inertia tensor **J** of a rigid body is defined as

$$\mathbf{J} = \begin{bmatrix} J_{xx} & J_{xy} & J_{xz} \\ J_{yx} & J_{yy} & J_{yz} \\ J_{zx} & J_{zy} & J_{zz} \end{bmatrix} \tag{A.1}$$

where each diagonal component of the inertia tensor **J** is defined as

$$\begin{aligned} J_{xx} &= \int_V \left(y^2 + z^2\right) dm \\ J_{yy} &= \int_V \left(x^2 + z^2\right) dm \\ J_{zz} &= \int_V \left(x^2 + y^2\right) dm \end{aligned} \tag{A.2}$$

and each extra-diagonal component is defined as

$$\begin{aligned} J_{xy} = J_{yx} &= -\int_V xy \cdot dm \\ J_{xz} = J_{zx} &= -\int_V xz \cdot dm \\ J_{yz} = J_{zy} &= -\int_V yz \cdot dm \end{aligned} \tag{A.3}$$

where V is the volume of the body, dm is the generic mass particle, x, y, z are the coordinates defining the spatial position of the generic mass particle in an orthogonal right-handed reference system.